Charge Dispersion and Recoil Properties at $A = 131$ from the Interaction of ^{238}U with 11.5-GeV Protons*

Yu-Wen Yu and N. T. Porile
Department of Chemistry, Purdue University, West Lafayette, Indiana 47907
(Received 24 October 1972)

Independent and cumulative yields have been measured for eight $A = 131$ nuclides formed in the interaction of ^{238}U with 11.5-GeV protons. A good fit to the cross sections was obtained with a charge dispersion consisting of two overlapping Gaussians peaking at $Z = 52.2$ and 56.5. The neutron-excessive curve accounts for about 40% of the total isobaric yield of 23.3 ± 0.4 mb. Thick-target recoil properties were determined for all the nuclides. The recoil ranges are characteristic of fission fragments for ^{131}Sb through ^{131}Cs but decrease by a factor of 2 between ^{131}Cs and ^{131}La. This decrease occurs some two Z units beyond the minimum between the two humps in the charge dispersion. The deposition energies derived from the recoil data exhibit a similar trend as the ranges, increasing in the manner expected for fission products up to barium but not beyond. The transformation of isotopic to isobaric yield distributions is considered and it is concluded that the use of N/Z as the composition variable gives the best agreement with experiment.

I. INTRODUCTION

The study of nuclear charge dispersion in the interaction of GeV protons with heavy elements has been of considerable interest in recent years. Charge-dispersion curves determined for the interaction of 3–28-GeV protons with uranium have been found to be unexpectedly complex. The curves range from near Gaussian at $A = 72$,[1] to single peaked and asymmetric, or perhaps double peaked, at $A \sim 109$,[2] $A = 111$,[3] and $A = 117$,[4] to double peaked at $A \sim 130$,[5,6] and $A \sim 147$,[7] to single peaked but now on the neutron-deficient side of stability at $A \sim 170$.[7] This behavior is in marked contrast to that observed at bombarding energies of several hundred MeV where the charge-dispersion curves are essentially Gaussian with maxima on the neutron-excessive side of stability.[5,8–11] These observations have usually been interpreted as reflecting the contribution of two or more mechanisms at GeV energies: fission, spallation, and fragmentation.

Recoil studies substantiate the results of the charge-dispersion measurements. At GeV energies the ranges of neutron-deficient products are approximately only half as large as those of neutron-excessive fission products of comparable atomic or mass numbers.[3,12–17] This situation does not hold at several hundred MeV where both neutron-deficient and -excessive products of similar mass number have comparable ranges of a magnitude characteristic of fission.[9,13–16,18,19] Beg and Porile[16] determined that this decrease in range occurs in a well-defined energy interval, 1–5 GeV. Differential range measurements performed at 2.2 GeV[20,21] confirm the difference in the magnitude of the ranges of neutron-excessive and -deficient products and also indicate that the latter have much broader range distributions extending down to very low values.

Although the nature of the charge dispersion of heavy elements at high energies appears to be understood in a general way, several problems remain. One disquieting feature of most experimental curves is that instead of being based on measurements on a single mass chain, they involve independent and cumulative yield determinations that may extend over a region of perhaps as many as 10 mass numbers. This approach has been followed because of the experimental difficulties inherent in measuring all or at least most of the independent yields at a given mass number. The complex shape of the charge dispersion at high energies, coupled with the fact that the isobaric yields extend over a wide range of atomic numbers on both sides of stability, makes such complete measurements necessary. While the determination of many independent and cumulative yields over a narrow mass range can adequately define the charge dispersion there are several problems in following this approach. These problems are related to the lack of knowledge about the variation with mass number of the parameters characterizing the charge dispersion. These parameters include the width of the curve, the peak or total cross section, and the distance of the most probable charge, Z_p, from the most stable charge at that mass number, Z_A. Moreover, since in the mass region $A = 110$–150 the charge dispersion consists of two distinct branches, it is neces-

sary to separately know the mass dependence of these parameters for each branch. In the absence of such detailed knowledge it is usually assumed that these parameters are invariant over the mass region of interest. This assumption can distort the measured curves in unknown ways. The only parameter which is known at least in a qualitative way is the mass dependence of the total isobaric yield associated with each branch, and corrections for this effect have in fact been made in recent measurements.[7]

Another open question is the extent of the correlation between charge dispersion and recoil ranges. Although it is true in a general way that neutron-deficient products from GeV bombardment of uranium have a much smaller range than neutron-excessive ones, it is not known whether the drop in range occurs at the exact minimum between the two branches of the charge dispersion. While it is conceptually attractive to ascribe both the occurrence of a double-peaked charge dispersion and the abrupt decrease in ranges to the same phenomenon, there is as yet no firm evidence that these two observations are that closely correlated.

In order to provide further information on these points we have performed a complete charge dispersion and thick-target recoil study on the $A = 131$ mass chain from the interaction of ^{238}U with 11.5-GeV protons. The study is complete in the sense that cumulative cross sections (c) and recoil properties have been determined for the effective end members of the chain, $^{131}_{51}Sb$ and $^{131}_{58}Ce$, and independent yields (i) and recoil properties have been obtained for the intervening six nuclides: $^{131m}_{52}Te$ and $^{131g}_{52}Te$, $^{131}_{53}I$, $^{131}_{54}Xe$, $^{131}_{55}Cs$, $^{131}_{56}Ba$, and $^{131}_{57}La$. As a check on the consistency of the results the cumulative yields and recoil properties of ^{131}I and ^{131}Ba were also measured.

II. EXPERIMENTAL

The experimental procedures used in this study were dictated by the decay properties and half-lives of the various isobars. The genetic relationship of the $A = 131$ isobars may be summarized as in Fig. 1. The Ba and Xe isomers play no role in this study and the independent yields of ^{131}Ba and ^{131}Xe include the respective contribution of these isomers. The direct decay of ^{131m}Ce to La has not been observed but a small branch cannot be ruled out.[22]

A. Targets and Irradiations

The target stack consisted of 20-μm uranium foil sandwiched between three pairs of 20-μm-thick aluminum foils of high purity (99.999%). The inner pair, immediately adjacent to the target, served as forward and backward recoil catchers, the middle pair as beam intensity monitors, and the outer pair as guard foils. All foils were cut to the same area, carefully aligned, and rigidly assembled by spark welding. Several irradiations of a stack including a 40-μm uranium foil, as well as of one consisting of only three aluminum foils, were also performed. These experiments served to determine the magnitude of secondary effects on both the $A = 131$ and monitor reaction yields. Prior to the assembly of the target stack, the uranium foil was cleaned with 6 N HNO_3 and various solvents, vacuum dried, and weighed.

The irradiations were performed with 11.5-GeV protons in the circulating beams of the zero gradient synchrotron (ZGS) and alternating gradient synchrotron (AGS) and ranged from 30 sec to 40 min in duration, depending on the half-life of the products of interest. After irradiation a 2×2 cm^2 portion of the target stack containing the most intensely irradiated region was cut for subsequent chemical or mass spectrometric analysis.

B. Separation Procedures

1. *Ba(c)-Cs-I(c) Series*

Target and catcher foils were separately dissolved in *aqua regia* in the presence of carriers in a vessel equipped with an iodine vapor trap. Several oxidation-reduction cycles were performed to ensure complete exchange between radioiodine and the added carrier. The above elements were sequentially separated from the solution by precipitation of barium as $BaCO_3$, extraction of I_2 into CCl_4, and precipitation of Cs as $Cs_3Bi_2I_9$. Standard procedures were used for further purifications and chemical yields were determined gravimetrically.

2. *Ce-La-Ba Series*

Target and catcher foils were rapidly dissolved in acid to which $HgCl_2$ had been added for greater dissolution speed. In addition to carriers, the dissolving solution contained ^{144}Ce and ^{140}La tracers which were subsequently used for chemical yield determinations as well as to check for cross contamination. (The production of these nuclides by reactions with uranium is negligible compared to the amount of added tracer.) The elements were sequentially separated from the solution by precipitation of $Ba(NO_3)_2$, $Ce(IO_3)_4$, and $La_2(C_2O_4)_3 \cdot 9H_2O$ following extraction of La^{+3} into TBP. All separation times were noted in order to permit subsequent decay and growth corrections. The Ba samples were purified immediately. The Ce and La samples were allowed to stand for some 7 h to permit complete decay of ^{131}Ce and ^{131}La to ^{131}Ba

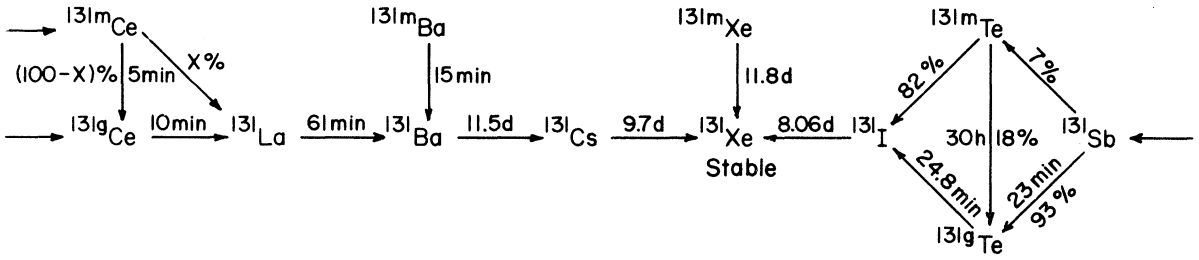

FIG. 1. Genetic relationship of the $A = 131$ isobars.

and, after chemical yield determination, were dissolved in the presence of Ba carrier and barium was separated and purified.

3. *Sb-Te-I Series*

Target and catcher foils were rapidly dissolved in concentrated HCl to which had been added NaOCl and $HgCl_2$ to promote dissolution. It was established in separate experiments that under these conditions $\geq 97\%$ of the iodine was formed in the I^- valence state rendering the time-consuming oxidation-reduction cycles unnecessary. First, antimony was separated by precipitation of Sb_2S_3 following extraction of Sb(V) into isopropyl ether-benzene solution in the presence of bromine water and back extraction of Sb(III) into 1 *N* HCl containing $NH_2OH \cdot HCl$. Iodine was separated from the aqueous phase by extraction into CCl_4 following the dropwise addition of $NaHSO_3$. Te was separated by reduction to the metal with SO_2. The Sb_2S_3 sample was set aside for several days to permit complete decay of ^{131}Sb to ^{131}I. The chemical yield of antimony was determined by assay of ^{124}Sb tracer which had been added to the dissolving solution. The chemical yield of Te was determined gravimetrically. The sample was allowed to stand for 3 h after which it was dissolved in the presence of iodine carrier and I was separated and purified. This sample contained the entire yield of ^{131g}Te and nearly none of the ^{131m}Te yield. The latter was determined by a subsequent iodine milking performed several days after irradiation.

4. *Xenon*

^{131}Xe was determined mass spectrometrically as part of a separate study of xenon isotopic cross sections and recoil properties.[23] Details of the experimental procedure are given elsewhere[23] and are essentially the same as those described in a previous measurement of xenon cross sections in high-energy reactions.[24]

C. Radioactivity Measurements

In order to minimize the errors associated with γ-ray branching ratios and detector efficiency, advantage was taken, whenever possible, of the

TABLE I. Decay properties of observed nuclides (Ref. 25).

Nuclide	Half-life	Radiation measured	Radiation abundance (%)	Method of detection
^{131m}Ce	5 min [a]	^{131}Ba 0.216-MeV γ	19	Ge(Li)
^{131g}Ce	10 min [a]	^{131}Ba 0.216-MeV γ	19	Ge(Li)
^{131}La	61 min [b]	^{131}Ba 0.216-MeV γ	19	Ge(Li)
^{131}Ba	11.5 day [c]	0.216-MeV γ	19	Ge(Li)
^{131}Cs	9.7 day	*K* x ray	88 [d]	NaI(Tl)
^{131}Xe	Stable			Mass spectrometer
^{131}I	8.06 day [e]	0.364-MeV γ	82	Ge(Li)
^{131m}Te	30 h	^{131}I 0.364-MeV γ	82	Ge(Li)
^{131g}Te	24.8 min	^{131}I 0.364-MeV γ	82	Ge(Li)
^{131}Sb	23 min	^{131}I 0.364-MeV γ	82	Ge(Li)
^{24}Na	14.96 h	1.369-MeV γ	100	Ge(Li)

[a] Reference 22.
[b] A. Spalek, I. Rezanka, J. Frana, J. Jursik, and M. Vobecky, Nucl. Phys. 118, 161 (1968).
[c] J. Fechner, A. Hammesfahr, A. Kuge, S. K. Sen, H. Toschinski, J. Voss, P. Weigt, and B. Martin, Nucl. Phys. 130, 545 (1969).
[d] Fluorescence yield.
[e] G. Graeffe and W. B. Walters, Phys. Rev. 153, 1321 (1967).

genetic relationship between the various isobars. The assays of ^{131}Ce and ^{131}La, as well as of ^{131}Ba(i) and ^{131}Ba(c), were performed on the ^{131}Ba decay product. Similarly the ^{131}Sb, ^{131}Te, ^{131}I(i), and ^{131}I(c) measurements were performed on ^{131}I. The disintegration rates of these nuclides were determined by γ-ray spectrometry performed with an accurately calibrated Ge(Li) detector operated in conjunction with a 1024-channel analyzer. The disintegration rate of ^{24}Na from the ^{27}Al($p, 3pn$) monitor reaction was also determined in this manner. Table I summarizes the decay properties on which our measurements were based and identifies the source of this information.

The nuclide ^{131}Cs decays 100% by electron capture to the ground state of ^{131}Xe making it impossible to determine its disintegration rate by the same method. Instead, the assay was performed by x-ray spectrometry with a thin NaI(Tl) detector. The detector was calibrated for xenon x rays with ^{132}Cs, ^{136}Cs, and ^{137}Cs sources which had been standardized by measurement of their known γ rays[25] with the same Ge(Li) detector used in the other radioactivity measurements. In this fashion the relative errors due to detector efficiencies were minimized.

One major difficulty in obtaining the ^{131}Cs disintegration rates is that the cesium samples also contained 6.5-day ^{132}Cs and 13-day ^{136}Cs, whose decay also involves x-ray emission. It was impossible to determine the contribution due to 9.7-day ^{131}Cs by decay curve analysis and the following procedure was adopted. Pure ^{132}Cs and ^{136}Cs sources were, respectively, prepared by the ^{133}Cs($n, 2n$) and ^{139}La(n, α) reactions induced by 14-MeV neutrons. The ratio of counting rates of the prominent γ rays (0.668 MeV for ^{132}Cs, 0.818 MeV for ^{136}Cs) to x rays was determined for each nuclide using the same γ-ray and x-ray detectors as in the high-energy study. Thereafter, all cesium samples were assayed with both detectors and the contribution of ^{132}Cs and ^{136}Cs to the x-ray spectra was subtracted by means of the measured γ-ray spectra and the previously determined x/γ ratios. Decay curve analysis[26] of the corrected x-ray activities gave very good least-squares fits on the assumption of two components, 32.1-h ^{129}Cs and 9.7-day ^{131}Cs, and a very small and essentially constant background (2.06-yr ^{134}Cs and 30.1-yr ^{137}Cs).

III. RESULTS

The activities at separation time or at end of bombardment were converted to disintegration rates by use of the radiation abundances, counting efficiencies, and chemical yields after correction of the cesium data in the manner outlined above. Various measurements performed with calibrated ^{131}Ba and ^{131}I sources indicated that no corrections were required for γ-γ or γ–x-ray summing effects.

Cross sections were obtained from the disintegration rates on the basis of a value of 8.6 mb[27] for the cross section of the ^{27}Al($p, 3pn$) monitor reaction. The cross sections for independent formation required in all cases corrections for growth and decay of progenitors during irradiation and up to the time of parent-daughter separation. These corrections were made by application of standard relationships. The calculation of the Ce, La, and Ba cross sections involves some unusual complications and this decay chain is considered in further detail in a separate section. The cross sections were also corrected for the effect of secondary reactions on the yields of the neutron-excessive products and of ^{24}Na and the results of experiments performed to determine the magnitude of this correction are given below.

A. Corrections for Secondary Effects

It is a well-known fact that the cross sections of products from high-energy reactions that are also formed in good yield in reactions induced by low-energy particles, especially neutrons, require corrections for secondary effects. The cross section of the ^{27}Al($p, 3pn$) reaction as well as those for the formation of the $A = 131$ neutron-excessive isobars fall in this category because of the importance of the ^{27}Al(n, α) reaction and of low-energy fission, respectively.

The secondary effect on the ^{27}Al($p, 3pn$) reaction was determined by measurement of the ^{24}Na/^{18}F disintegration-rate ratio. This ratio was determined in upstream and downstream monitors from target stacks containing 20- or 40-μm uranium foils. The correct ratio, free from secondary effects, was determined in the irradiation of a target stack consisting of three 20-μm-thick aluminum foils of which the middle one was assayed. This procedure is based on the assumptions that the formation of ^{18}F from aluminum is free of secondary effects and that the aluminum stack is sufficiently thin to make the secondary production of ^{24}Na completely negligible. Previous studies of the secondary effect on the monitor reaction cross section[28,29] indicate that these assumptions are valid.

The results of these experiments are summarized in Table II which also includes an extrapolation to 100 mg/cm^2 of uranium. The quoted uncertainties are standard deviations based on three separate determinations. It is seen that the effect

TABLE II. Secondary effect on the production of ^{24}Na and $A = 131$ nuclides.

Product	Percentage secondary effect 20-μm U (38 mg/cm^2)	40-μm U (76 mg/cm^2)	100 mg/cm^2 U
^{24}Na (upstream)	4.7 ± 0.4	9.2 ± 1.6	12.2 ± 2.1
^{24}Na (downstream)	6.2 ± 0.6	12.5 ± 2.0	16.7 ± 2.7
^{131}I	10.4 ± 1.4		27.2 ± 3.8
^{131g}Te	12.1 ± 2.7		31.8 ± 7.2
^{131m}Te	13.3 ± 2.1		34.8 ± 5.3
^{131}Sb	16.4 ± 1.6		42.3 ± 4.2

increases in essentially linear fashion with target thickness. As expected from the predominantly forward motion of second particles, the effect on the downstream monitor is somewhat larger than that on the upstream one. While this result confirms that it is indeed preferable to monitor the beam intensity with the upstream foil, the correction for the latter is still nearly 5% for a 20-μm-thick target.

Chu, Franz, and Friedlander[30] have recently performed similar measurements at 28 GeV. Their results for 100 mg/cm^2 uranium are 12.4 ± 1.4% and 15.6 ± 1.4% for the upstream and downstream monitors, respectively, in good agreement with the present data.

The secondary effect on the yields of the neutron-excessive products was determined by measurement of the cross sections with 20- and 40-μm-thick target foils on the assumption that the effect varies linearly with target thickness. The results are summarized in Table II where the quoted uncertainties represent standard deviations based on several determinations for each thickness. The secondary effect for a 20-μm-thick target is seen to range between 10 and 16%. Comparable results have been obtained by Chu, Franz, and Friedlander[30] for various neutron-excessive nuclides formed in 28-GeV bombardment of uranium.

It should be stated that all the secondary effect measurements were made at the ZGS but the results were equally applied to the AGS bombardments. Although small differences in the magnitude of the effect might be expected because of differences in beam profile and radial attenuation, the close agreement between our data and the AGS results of Chu, Franz, and Friedlander[30] indicates that the difference due to accelerator characteristics may be neglected.

B. Problem of ^{131}Ce

The ^{131}Ce isomers present a special problem. Because of their short half-lives, 5 and 10 min, we were only able to perform a single separation of ^{131}Ce from its decay products per experiment. Since the isomer ratio is unknown, the total ^{131}Ce production cross section is rendered uncertain. Furthermore, since a sizable fraction of ^{131}Ce de-

TABLE III. Dependence of Ce, La, and Ba yields on the Ce isomer ratio and the direct decay of ^{131m}Ce to ^{131}La.

Nuclide	100% ^{131g}Ce [a] (mb)	100% ^{131m}Ce [b] (mb)	σ [c] (mb)	$+1\sigma$ [d] (mb)	10% ^{131}La [e] (mb)
^{131m}Ce	0.00	3.41	2.16	2.56	2.35
^{131g}Ce	4.15	0.00	1.58	1.10	1.55
^{131}Ce	4.15	3.41	3.72	3.66	3.90
^{131}La	1.72	3.80	3.00	3.23	2.80
^{131}Ba	2.66	2.39	2.50	2.47	2.52
Sum	8.53	9.60	9.22	9.36	9.22
^{131}Ba(c) (Experimental)		9.22 ± 0.14			

[a] Calculation assumes 100% yield of ^{131g}Ce.
[b] Calculation assumes 100% yield of ^{131m}Ce.
[c] Yields whose sum gives exact agreement with σ_c (Ba).
[d] Yields whose sum differs from σ_c (Ba) by 1 standard deviation.
[e] Yields whose sum gives exact agreement with σ_c (Ba) for a 10% direct decay branch of ^{131m}Ce to ^{131}La.

TABLE IV. Formation cross sections of $A=131$ isobars from 11.5-GeV proton bombardment of uranium.

Present results at 11.5 GeV and zero target thickness				Previous results		
Product	Number of replicate determinations	Type of yield [a]	σ (mb)	E_p (GeV)	Formation cross section (mb)	Target thickness (μm)
^{131}Ce	4	C	3.72±0.24			
^{131}La	4	I	3.00±0.14			
^{131}Ba	5	C	9.22±0.14	6	6.6±0.9 [b]	40
				11.5	8.8±0.1 [c]	20
^{131}Ba	4	I	2.50±0.26			
^{131}Cs	4	I	2.32±0.06	6	2.4±1.1 [b]	40
				24	2.02±0.05 [d]	Thin
^{131}Xe	4	I	2.48±0.30	29	2.5±0.6 [e]	40
^{131}I	4	C	9.09±0.47	18	13.1±1.3 [f]	20 or 40
^{131}I	5	I	3.10±0.15	18	3.51±0.28 [f]	20 or 40
^{131g}Te	4	I	1.53±0.15			
^{131m}Te	4	I	2.44±0.17	18	3.2±1.0 [f]	20 or 40
^{131}Sb	5	C	2.39±0.09	18	2.36±1.1 [g]	40

[a] C=cumulative, I=independent.
[b] Reference 5.
[c] Reference 16.
[d] Reference 33.
[e] Reference 24.
[f] Reference 32.
[g] Reference 31.

cays during irradiation and prior to separation, this uncertainty extends to the ^{131}La cross section and, to a much smaller extent, to the ^{131}Ba cross section. A further complication arises from the fact that the decay properties of the 5-min ^{131}Ce isomer are not completely known. Norris, Friedlander, and Franz[22] discovered this isomer and studied its decay properties. While they found evidence of an isomeric transition to the 10-min ground state they were unable to rule out direct decay to ^{131}La. As shown below, this adds a further uncertainty to the ^{131}Ce and ^{131}La cross sections.

It fortunately turns out that the sum of the ^{131}Ce, ^{131}La, and ^{131}Ba cross sections, as well as the individual values, depend on the assumptions made about the ^{131}Ce isomer ratio. The measured cumulative cross section of ^{131}Ba which is equal to this sum, thus provides an effective constraint on the relative yield of the ^{131}Ce isomers thereby allowing a rather unambiguous determination of the ^{131}Ce, ^{131}La, and ^{131}Ba cross sections.

The complete set of radioactive growth and decay expressions for these nuclides was coded for computer evaluation of the cross sections on the basis of the measured disintegration rates and irradiation and separation times for a variety of assumptions concerning ^{131}Ce. The results of the calculations are summarized in Table III. Columns 2 and 3 give the results for two interesting limiting cases: 100% yield of ^{131g}Ce and 100% yield of ^{131m}Ce, respectively, with no direct decay of the latter to ^{131}La. The difference between the two sets of values is the net result of a number of factors in the growth-decay equations. It is seen that the sum of the Ce, La, and Ba cross sections is 13% larger on the assumption that cerium is formed as ^{m}Ce rather than as ^{g}Ce. The measured cumulative cross section of ^{131}Ba is 9.22±0.14 mb. This value lies between the calculated ones indicating that both cerium isomers are formed. Column 4 gives the results for an isomer ratio of 1.37, a value that leads to exact agreement with the ^{131}Ba(c) cross section. As might be expected, the various cross sections lie between the limiting values given in the first two columns. As an indication of the accuracy of this procedure, column 5 lists the cross sections whose sum is 9.36 mb, a value that differs from the measured ^{131}Ba(c) yield by 1 standard deviation. It is seen that the uncertainty in the cross sections arising from this analysis ranges from 1% for ^{131}Ba to 8% for ^{131}La.

The occurrence of positron or electron capture decay of ^{131m}Ce would lead to a larger cross section for this isomer and to a smaller one for ^{131}La, leaving all the other cross sections nearly unchanged. The effect of a 10% direct decay branch is illustrated in column 6 of Table III. The total ^{131}Ce cross section is seen to increase by about 4% while that of ^{131}La decreases by approximately 7%. The magnitude of this effect varies nearly linearly with the branching ratio.

C. Cross-Section Results

The corrected cross sections are tabulated in Table IV. The values given for Ce, La, and Ba are those calculated on the assumption of 100%

isomeric decay of ^{131m}Ce. The quoted uncertainties are standard deviations based on the agreement between replicate determinations. The uncertainties quoted for Ce, La, and Ba have been increased to reflect the possible errors resulting from the analysis described in the preceding section. Additional systematic uncertainties arising from detector efficiencies and branching ratios are expected to be small ($\leq 5\%$) particularly with respect to the relative isobaric yields. The absolute uncertainty in the ^{131}Xe cross section is somewhat larger (15%) because of the different method of determination.

A check on the consistency of the results obtained for the neutron-excessive products can be made by comparing the ^{131}I(c) cross section with the sum of the ^{131}I(i), $^{131m+g}$Te(i), and ^{131}Sb(c) yields. The sum of the latter values is 9.46 ± 0.31 mb in good agreement with the cumulative cross section of 9.09 ± 0.47 mb.

The separate measurement of the independent yields of both ^{131}Te isomers determines the Te isomer ratio. The result is 1.60 ± 0.22 with the high-spin isomer being favored. This result is in accord with the well-established fact[31] that high-spin isomers are consistently favored in high-energy fission.

A number of independent and cumulative yield measurements of $A = 131$ isobars formed in the interaction of uranium with GeV protons have been reported.[5, 16, 24, 31-33] The results obtained at 6–29 GeV are summarized in Table IV. Most of these results do not include corrections for secondaries and no attempt has been made to make such corrections. The comparison is in any case approximate, since practically none of the literature values are based on 11.5-GeV bombardments. The agreement is in most instances reasonably good. It does appear, however, that the values obtained by Rudstam and Sørensen[32] for ^{131m}Te(i), ^{131}I(i), and ^{131}I(c) are systematically larger than the present results. Also, the value reported by Friedlander *et al.*[5] for ^{131}Ba(c) appears to be somewhat low.

D. Total Isobaric Cross Section at $A = 131$

The total isobaric cross section may be obtained by addition of the Cs and Xe independent yields, the ^{131}Ba cumulative yield, and an average of the ^{131}I cumulative yield and the sum of the appropriate independent yields. The result is 23.3 ± 0.4 mb, exclusive of systematic errors. Other determinations of this quantity at multi-GeV energies include a value of 23.5 ± 2 mb obtained by Hudis *et al.*[24] at 29 GeV and an estimate of 28 ± 3 mb at 3 GeV due to Friedlander.[6]

E. Recoil Properties

The quantities determined in the recoil experiments are the fraction of the total activity of a given nuclide collected in the forward and backward catchers, denoted by F and B, respectively. The recoil properties of interest are the experimental range, $2W(F+B)$, and the forward-to-backward ratio, F/B. The target thickness is denoted by W. These quantities are summarized

TABLE V. Corrected recoil properties of observed nuclides.

	Present results at 11.5 GeV				Previous results		
Product	Number of determinations	Type of yield [a]	$2W(F+B)$ (mg/cm^2)	F/B	E_p (GeV)	$2W(F+B)$ (mg/cm^2)	F/B
^{131}Ce	4	C	2.91 ± 0.32	1.29 ± 0.09			
^{131}La	4	I	3.10 ± 0.33	1.39 ± 0.12			
^{131}Ba	5	C	3.47 ± 0.15	1.30 ± 0.06	11.5	3.58 ± 0.11 [b]	1.27 ± 0.02
^{131}Ba	4	I	5.28 ± 0.20	1.28 ± 0.16			
^{131}Cs	4	I	6.95 ± 0.31	1.12 ± 0.09			
^{131}Xe	3	I	7.77 ± 0.97	1.23 ± 0.09			
^{131}I	4	C	8.25 ± 0.20	1.06 ± 0.02	18	8.5 ± 1.3 [c]	0.97 ± 0.17
					6	8.1 [d]	1.16
^{131}I	5	I	7.34 ± 0.60	1.11 ± 0.07			
^{131g}Te	4	I	8.63 ± 1.15	1.24 ± 0.07			
^{131m}Te	4	I	8.36 ± 0.98	1.09 ± 0.03			
^{131}Sb	4	C	8.24 ± 0.70	1.03 ± 0.07			
Ce + La + Ba (weighted)			3.61 ± 0.50	1.32 ± 0.23			
Sb + Te + I (weighted)			8.04 ± 1.77	1.10 ± 0.14			

[a] C = cumulative, I = independent.
[b] Reference 16.
[c] Reference 14.
[d] Reference 13.

in Table V and include a 3% correction for scattering.[18] The quoted uncertainties are standard deviations based on the agreement between the indicated number of replicate determinations. The main sources of these uncertainties, particularly for the short-lived products, are the corrections for progenitor decay and for differences in separation time between the three samples comprising a given recoil measurement. The recoil data have not been corrected for secondary effects. The fact that the recoil properties of neutron-excessive products are nearly independent of energy[16] makes such corrections unnecessary.

The results for ^{131}Ba(c) and ^{131}I(c) provide a check on the consistency of the data. The results for the independent formation of Ce-La-Ba and Sb-Te-I have been weighted by the respective formation cross sections and summed for comparison with the cumulative data. The resulting values are listed in Table V and are seen to be in good agreement with the cumulative data.

The recoil properties of ^{131}I(c) and ^{131}Ba(c) have been measured at 6–18 GeV by a number of workers.[13, 14, 16] The ranges and F/B values reported in the literature are summarized in Table V and are generally in good agreement with the present values.

IV. DISCUSSION

A. Parametrization of the Charge Dispersion

The determination of eight independent or cumulative yields at $A = 131$ provides rather detailed information about the charge dispersion at this mass number. The occurrence of two maxima in the isobaric yields suggests a parametrization of the charge dispersion in terms of two Gaussians. A nonlinear least-squares program was used to fit the measured cross sections by the expression:

$$\sigma_I(Z) = \sigma_{\max(\mathrm{ne})} \exp\{-[Z - Z_p(\mathrm{ne})]^2/2S^2(\mathrm{ne})\} + \sigma_{\max(\mathrm{nd})} \exp\{-[Z - Z_p(\mathrm{nd})]^2/2S^2(\mathrm{nd})\}, \quad (1)$$

where the quantities indexed by (ne) refer to the neutron-excessive Gaussian and those indexed by (nd) to the neutron-deficient one. The procedure involved a number of iterations in which the independent yields of Sb and Ce were first estimated and then adjusted to meet the constraints imposed by the Sb and Ce cumulative yields.

TABLE VI. Charge-dispersion parameters at $A = 131$.

	Neutron excessive	Neutron deficient
$\sigma_{\max}$ (mb)	3.81 ± 0.37	2.96 ± 0.25
σ_{tot} (mb)	9.88 ± 1.50	13.49 ± 1.70
Z_p	52.21 ± 0.13	56.46 ± 0.25
N/Z_p	1.509 ± 0.012	1.320 ± 0.021
FWHM	2.44 ± 0.25	4.28 ± 0.40

The resulting charge dispersion is shown in Fig. 2 and the Gaussian parameters are summarized in Table VI. The choice of two Gaussians is satisfactory in terms of the agreement with the data. In addition to adequately fitting the independent yields, the calculated dispersion is in accord with the cumulative yields. The values for ^{131}Sb and ^{131}Ce obtained from the curves thus are 2.39 and 3.70 mb, in agreement with the corresponding experimental values, 2.39 ± 0.09 mb and 3.72 ± 0.24 mb.

The over-all charge dispersion is seen to consist of a rather narrow neutron-excessive fission peak and a much broader neutron-deficient curve. The fission peak has a full width at half maximum (FWHM) of 2.4Z units, peaks in the vicinity of tellurium and accounts for approximately 40% of the total isobaric yield. The neutron-deficient curve peaks midway between barium and lanthanum and its FWHM is 4.3Z units. The two curves overlap to a substantial extent and the peak-to-valley ratio is only of the order of 2 to 1. Because of its great width the neutron-deficient curve contributes to a significant extent to products as neutron rich as iodine. The minimum between the two peaks lies nearly midway between Xe and Cs at $Z = 54.3$. Perhaps fortuitously, this is just equal to the value of Z_A at this mass number.

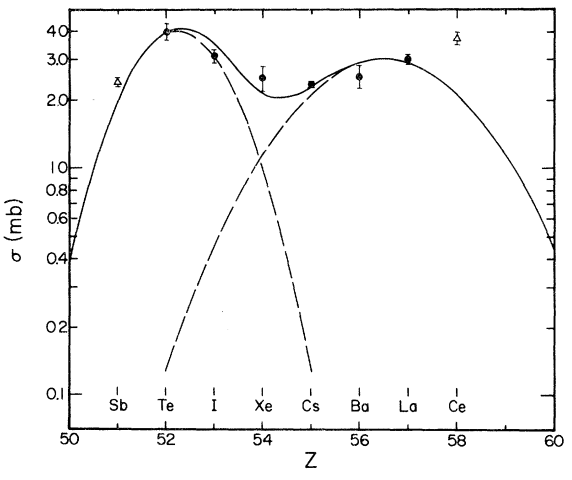

FIG. 2. Charge dispersion at $A = 131$ in the interaction of ^{238}U with 11.5-GeV protons. Solid points, measured independent yields; open points, measured cumulative yields. The dashed curves represent a two-Gaussian fit to the data and the solid curve is their sum.

B. Comparison with Isobaric and Isotopic Distributions

A number of relevant isobaric and isotopic yield distributions have been determined in the mass region of interest. Hogan and Sugarman[9] measured the charge dispersion at $A = 139$ in the fission of uranium by 0.45-GeV protons. At this energy the dispersion can be characterized by a single Gaussian and these workers obtained a curve peaking about $0.4Z$ units on the neutron-rich side of stability with FWHM $= 3.2Z$ units. While a strict measure of the energy dependence of the charge dispersion is not afforded by these data because of the difference in mass number, it is apparent that the present neutron-excessive curve is narrower and peaks at least one Z unit farther from stability. This behavior is contrary to the well-known trend with proton energy of increasing width and Z_p value of the charge dispersion. This trend has been noted up to bombarding energies of several hundred MeV and can be understood in terms of the increase in deposition energy and the proliferation of fissioning nuclei with increasing bombarding energy. The charge dispersion obtained for 28-GeV protons by Chu *et al.*[7] at $A \sim 147$ shows a similar departure from the trend noted at lower energies with respect to the value of $Z_A - Z_p$ although the width of their curve is about one Z unit larger than ours.

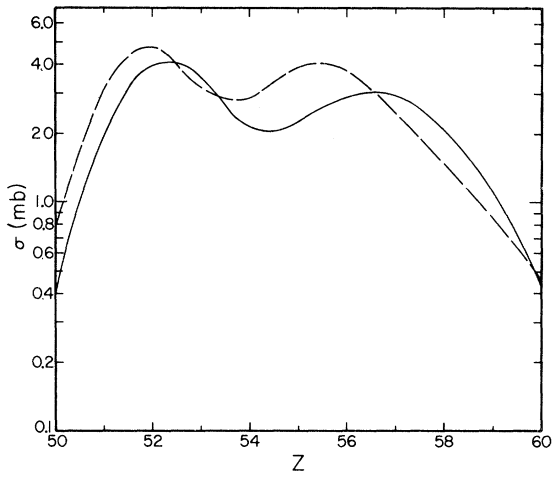

FIG. 3. Comparison of present charge dispersion (solid curve) with that determined by Friedlander *et al.* (Refs. 5 and 6) at 2.9 GeV (dashed curve).

The charge dispersion at $A = 131$ has been previously determined at 2.9 GeV[6] on the basis of independent and cumulative yields of various Cs and Ba isotopes[5] corrected for variation with A of the total isobaric yield over the mass region covered by the experimental data. The two charge dispersions are compared in Fig. 3. Although the two curves have a similar over-all shape there are substantial differences between them. Friedland-

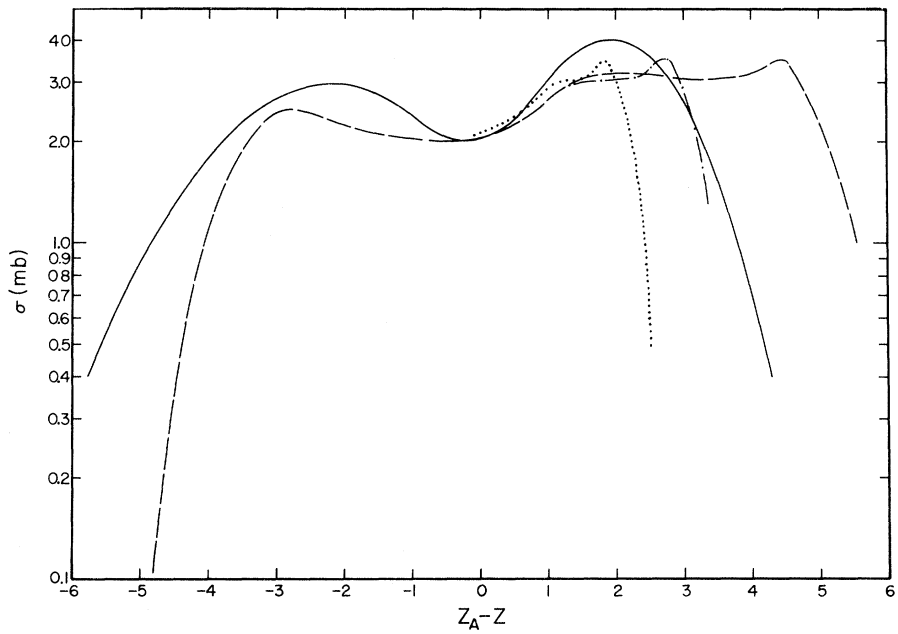

FIG. 4. Transformation of cesium isotopic distribution to isobaric distribution at $A = 131$. Solid curve, present charge dispersion; dashed, transformation due to Chu *et al.* (Ref. 7); dot-dashed, transformation with Z_A values uncorrected for shell effects; dotted, transformation corrected for variation of $Z_p - Z_A$ with A. Note that the use of $Z_A - Z$ as the abscissa reverses the position of the two peaks relative to Fig. 2.

er's curve is shifted towards the neutron-excessive side by $0.5Z$ units for the neutron-rich hump and by somewhat over $1Z$ unit for the neutron-deficient one. In addition, the reported cross sections on the near neutron-deficient side of stability are substantially larger than the present values. It is unfortunately not possible to determine to what extent these differences reflect the use of cross sections distributed over a range of mass numbers in the earlier work and to what extent they merely reflect the difference in bombarding energy.

In recent years it has become possible to measure isotopic yield distributions in high-energy reactions by use of on-line mass spectrometry. If a reliable procedure can be found to transform an isotopic into an isobaric distribution it may thus be possible to circumvent the difficulties inherent in charge dispersion measurements.

The independent yields of some 25 cesium isotopes from the interaction of uranium with 24-GeV protons have been determined by Chaumont.[33] Since this distribution is centered in the vicinity of $A = 131$ it may be used to obtain a charge dispersion for comparison with the present data. Such a comparison should be valid in spite of the difference in bombarding energies as it is known that the cross sections of complex reactions are nearly independent of energy in the 10–30-GeV range. Chaumont's data have, in fact, already been used for this purpose by Chu *et al.*[7] and the general procedure for making such a transformation is described in their work. The transformation involves a change in abscissa from A to a quantity appropriate to an isobaric distribution such as $Z_A - Z$ or N/Z. In addition, the isotopic cross sections should be corrected for possible variations in charge-dispersion parameters over the mass region covered by the isotopic yields, in this case $A = 119$–144.

Figure 4 shows the results of several transformations in which the cross sections are plotted as a function of $Z_A - Z$. The dashed curve is that obtained by Chu *et al.*[7] It features a correction for the mass dependence of the total cross section associated with each branch of the charge dispersion and the use of shell-corrected Z_A values. The shell correction becomes of importance beyond ^{137}Cs because of the closure at this point of the $N = 82$ shell. The transformed curve is in marked disagreement with the present charge dispersion except in the vicinity of the common ^{131}Cs point. The former thus extends some two Z units beyond the latter on the neutron-rich side but is about one Z unit narrower on the neutron-deficient side. In addition, there are discrepancies of some 30% in the region of the peaks. While the experimental curve is not uniquely defined in the region of the wings, the cumulative yields of ^{131}Ce and ^{131}Sb do provide sufficient constraints to make it extremely unlikely that such a large discrepancy can be attributed to an error in this curve.

Since the cesium points lie on both sides of the $N = 82$ shell, while the $A = 131$ points do not [except for a small contribution to the ^{131}Sb(c) yield], at least part of the discrepancy may reflect the discontinuity in Z_A values arising from shell closure. The dot-dashed curve in Fig. 4 represents a recalculation of Chu's curve based on Z_A values uncorrected for shell closure. Since the Z_A values corresponding to the mass numbers of the heaviest cesium isotopes are now smaller, the neutron-rich wing of the curve is compressed and is seen to be in much better agreement with experiment. This procedure does not, of course, affect the other discrepancies noted above. In order to bring the neutron-deficient wing of the transformed curve into agreement with experiment it is necessary to adjust the charge-dispersion parameters below $A \sim 124$. The neutron-deficient branch would thus have to be significantly narrower than at $A = 131$, or else be shifted towards stability. Presently available information on charge dispersions is not accurate or detailed enough to warrant such a correction.

A number of workers[8, 11, 18] have determined the variation of Z_p with A in the fission of uranium by 450-MeV protons. The results indicate that $Z_A - Z_p$ increases with A above $A \sim 133$. If these results are applicable at multi-GeV energies then the neutron-excessive part of the derived charge dispersion should be corrected for this effect. The dotted curve in Fig. 4 shows the effect of this correction on either one of the previously derived curves and the resulting charge dispersion is now much narrower than the experimental one. Evidently, as already apparent from the comparison with Hogan and Sugarman,[9] the neutron-excessive charge dispersion changes sufficiently over this energy interval to make the use of the 450-MeV data inappropriate.

In view of the poor agreement of the isotopic and isobaric data when plotted as a function of $Z_A - Z$ it seemed worthwhile to explore the usefulness of N/Z as a charge-dispersion variable. Although this parameter is not as appropriate to charge dispersions as one that varies linearly with Z it does eliminate the above mentioned problem of the discontinuity in Z_A at shell closure. Figure 5 shows a comparison of the cesium data, corrected for isobaric yield variation, and the $A = 131$ results on an N/Z plot. Although many discrepancies remain, it appears that this transformation gives the best over-all agreement between isotopic and

isobaric curves. This result may of course be only fortuitous and the situation may be different in other mass regions. In any case it can be concluded from this analysis that it is difficult to perform a really meaningful transformation of an isotopic to an isobaric distribution.

C. Charge Dispersion and Recoil Ranges

One of the purposes of this study was to determine if the transition between long and short ranges occurred at the same Z value as that between the neutron-excessive and -deficient branches of the charge dispersion. This question is considered in the present section.

The experimental ranges are plotted as a function of atomic number in Fig. 6. The ranges of cumulatively formed ^{131}Sb and ^{131}Ce are plotted at the corresponding effective Z values as obtained from the charge dispersion. The sharp decrease in ranges occurs between Cs and La and is centered at Ba. The behavior of the ranges expected from the charge dispersion can be obtained in a number of ways, all giving essentially the same result. The simplest set of assumptions is that the ranges of the neutron-excessive products are constant and equal to the average of the Sb and Te values while those of the neutron-deficient products are also constant and equal to the average of the La and Ce values. The dot-dashed curve in Fig. 6 is obtained by weighting these two range values by the relative contributions at each Z from the two branches of the charge dispersion. It can be seen that the curve differs markedly from the experimental ranges in that the decrease is centered at Xe, two Z units lower than observed.

A more realistic analysis, in which allowance is made for the slight variation in the ranges of isobaric fission fragments with Z, does not in the least alter this conclusion. The solid curve drawn through the experimental ranges shows the effect of a reduction in range of 4.3% per Z, a value determined by Hogan and Sugarman[9] at 450 MeV for a great number of fission products with $A \sim 139$. It is apparent that the Z dependence is consistent with fission through Xe but shows a marked deviation at Ba. The combination of this curve with either a constant value for the ranges of neutron-deficient products or with a line having a 4.3% decrease per Z, as obtained from the Ce and La data, again shows a transition centered at Xe, as indicated by the dashed curve.

A more basic, but less directly obtainable quantity than the range, is the kinetic energy of the fragment. The kinetic energies were obtained from the ranges by means of an analysis described in the next section. The use of these quantities for an analysis such as that shown in Fig. 6 leads to the same conclusion: There is a difference of two atomic numbers in the location of the transition point obtained from the charge dispersion and recoil data.

One can think of several explanations for the difference between these two types of measurements.

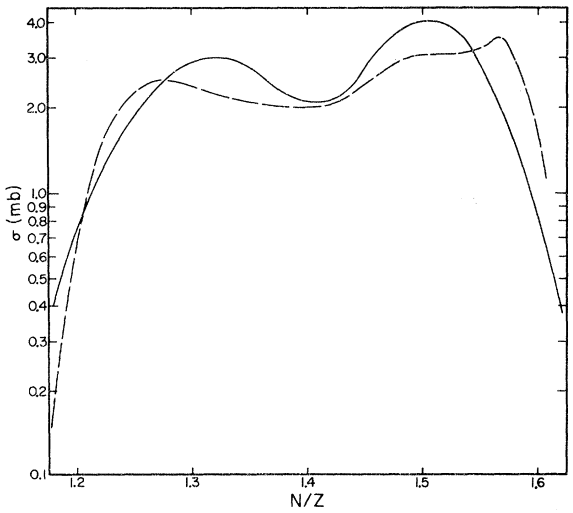

FIG. 5. Comparison of transformed cesium isotopic distribution (dashed curve) with present charge dispersion (solid curve) on an N/Z plot. Note that the use of this variable reverses the position of the two peaks relative to Fig. 2.

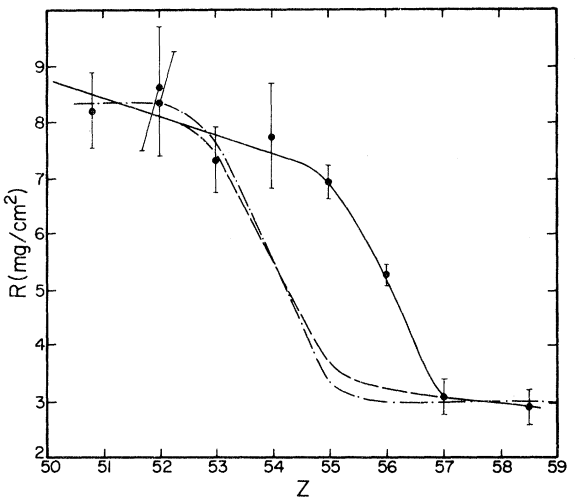

FIG. 6. Dependence of experimental ranges on product Z. The values for ^{131}Sb and ^{131}Ce are plotted at the appropriate effective atomic numbers obtained from the charge dispersion. Solid curve is drawn through experimental points and features a 4.3% per Z decrease for neutron-excessive products; dashed and dot-dashed curves signify trends expected from charge dispersion.

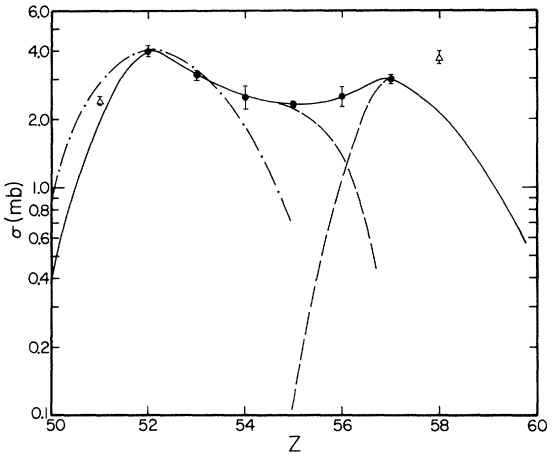

FIG. 7. Charge dispersion expected from recoil ranges and the assumption of two mechanisms. Solid curve is the charge dispersion drawn through experimental points; dashed curves derived from recoil data; dot-dashed curve is the neutron-excessive curve obtained at $A = 147$ (Ref. 7) normalized in height and peak position.

The one that is perhaps conceptually most attractive, in that it retains the notion of two distinct mechanisms each characterized by a given charge dispersion and recoil properties, is that the peaks of the charge dispersion are not Gaussian. Although the assumption of a Gaussian charge dispersion in fission has been found to be valid up to several hundred MeV, there is no guarantee that this remains the case at multi-GeV bombarding energies. Furthermore, there is really no justification for a neutron-deficient Gaussian other than that it fits the data. It thus makes some sense to turn the question around and let the recoil ranges determine the shape of the charge dispersion. For this purpose the ranges of fission products were assumed to decrease by 4.3% per Z unit and the actual values obtained from a least-squares fit to the Sb, Te, I, and Xe ranges. The ranges of neutron-deficient products were assumed to have a similar behavior as indicated by the La and Ce values. The measured ranges of Cs and Ba lie between these two sets of values and the contributions from each mechanism were taken as equal to those of the corresponding range values.

The resulting charge dispersion is shown in Fig. 7 where the curve drawn through the experimental points has been decomposed in the above manner. The neutron-rich curve is now very broad and asymmetric with FWHM of the order of $4Z$ units. The neutron-deficient curve is much narrower than before and somewhat asymmetric. An interesting comparison can be made with the charge dispersion at $A \sim 147$ reported by Chu *et al.*[7] They find that at this higher mass number the two humps of the charge dispersion are more completely separated so that their shape can be defined without assuming a parametrization. Their reported curves are essentially Gaussian with perhaps some tailing between them. The vast difference between the shapes of the neutron-excessive curves can be seen in Fig. 7, where the curve for $A \sim 147$ has been superimposed on the curve under consideration. In view of this difference it seems unlikely that the charge-dispersion curve based on the ranges can be valid unless there is a drastic change in shape between $A = 131$ and 147. It would be of interest to determine the dependence of the recoil ranges on Z at $A \sim 147$ because of the clear separation between the two branches of the charge dispersion. Some data in this region have in fact been reported recently by Cumming and Bächmann.[17] However their results do not sufficiently cover the $Z_A - Z$ region of importance to indicate the degree of correlation between ranges and charge dispersion.

On the other hand, if the Gaussian decomposition of the charge dispersion is regarded as being essentially correct[7] the situation becomes rather complex. Under these conditions fission accounts not only for the neutron-excessive peak but its contribution extends all the way up to the maximum of

TABLE VII. Recoil parameters of $A = 131$ isobars.

Nuclide	R_0 (mg/cm^2)	$\eta_{\parallel}$	T (MeV)	$v_{\parallel}$ (MeV/amu)$^{1/2}$	E^* (MeV)
^{131}Ce	2.90 ± 0.31	0.0501 ± 0.0136	18.9 ± 1.7	0.0269 ± 0.0074	143 ± 39
^{131}La	3.07 ± 0.33	0.0648 ± 0.0167	20.2 ± 1.9	0.0360 ± 0.0094	191 ± 50
^{131}Ba	5.26 ± 0.20	0.0486 ± 0.0228	34.9 ± 1.5	0.0354 ± 0.0167	189 ± 89
^{131}Cs	6.94 ± 0.31	0.0276 ± 0.0195	49.5 ± 2.8	0.0240 ± 0.0170	128 ± 90
^{131}Xe	7.74 ± 0.97	0.0407 ± 0.0143	57.8 ± 9.6	0.0383 ± 0.0138	204 ± 73
^{131}I	7.33 ± 0.60	0.0254 ± 0.0153	54.8 ± 5.8	0.0232 ± 0.0141	124 ± 75
^{131g}Te	8.60 ± 1.15	0.0423 ± 0.0110	68.7 ± 12.6	0.0434 ± 0.0120	231 ± 64
^{131m}Te	8.36 ± 0.98	0.0210 ± 0.0067	66.1 ± 10.5	0.0211 ± 0.0069	112 ± 37
^{131}Sb	8.24 ± 0.70	0.0072 ± 0.0165	66.0 ± 7.6	0.0072 ± 0.0166	38 ± 88

the neutron-deficient peak. Fission, in fact, then accounts for about $\frac{1}{3}$ of the total cross section associated with this peak. The occurrence of a minimum in the charge dispersion is then rather puzzling since fission is the dominant mechanism on both sides of this point. The explanation of this feature presumably lies in the details of the competition between spallation and fission in the particular distribution of excited residual nuclei resulting from the interaction of ^{238}U with 12-GeV protons. In the absence of detailed Monte Carlo calculations at this energy one can speculate that the probability of a fission process leading to neutron-excessive and neutron-deficient products is appreciably larger than that of fission leading to products near stability. Since, as discussed in the next section, the atomic number of isobaric fission products is related to the deposition energy of the residual nuclei produced in the intranuclear cascade, this statement implies that the probability of fission following cascades leading to intermediate deposition energies is low compared to that following cascades leading to low or high deposition energies. A similar viewpoint has recently also been advanced by Starzyk and Sugarman.[34]

D. Recoil Parameters

The two-step velocity vector model may be used to extract the following recoil parameters from the measured recoil properties: the range of the fragment in the moving frame R_0, the corresponding kinetic energy T, the ratio of impact to breakup velocities $\eta_{\|}$, the component of the impact velocity along the beam direction $v_{\|}$, and the average deposition energy of the residual nuclei leading to the products of interest E^*. The particular formulation of the vector model used in this analysis as well as the choice of range-energy relations has been described in detail elsewhere.[35]

The derived recoil parameters are summarized in Table VII. The kinetic energies of the fragments exhibit a gradual decrease with increasing Z up to cesium followed by a sharp decrease between Cs and La. This behavior closely mirrors that of the ranges and confirms the above-mentioned discrepancy between the charge dispersion and recoil data.

A quantity of special interest to an understanding of high-energy reactions is the deposition energy. It has been shown by a number of workers, most notably by Hogan and Sugarman,[9] that the E^* values leading to the formation of high-energy fission products increase with Z along an isobaric chain. This behavior is a well understood consequence of the need of higher excitation energies to permit the evaporation of more neutrons in order to form increasingly more neutron-deficient products. Hogan and Sugarman find that the increase in E^* amounts to some 35 MeV per Z for a wide range of nuclides with $A \sim 139$ in the 450-MeV proton fission of uranium. The deposition energies derived in the present work are plotted in Fig. 8 and the 35 MeV/Z trend is fitted to the values for the neutron-excessive products. It is seen that, within the rather large uncertainties of the E^* values, the trend expected for a fission process is followed by the $A = 131$ isobars up to barium at which point the values deviate from the trend. The same conclusion still holds if a 30 MeV/Z trend obtained by Cumming and Bächmann,[17] in a reanalysis of the data of Hogan and Sugarman[9] is imposed on our data. This type of behavior has been attributed[13, 16, 36] to a breakdown of the two-step model of high-energy reactions resulting from the massive onset of a fragmentation process.

V. CONCLUSIONS

Independent or cumulative yields and recoil properties have been measured for eight nuclides having $A = 131$. A good fit to the yields can be obtained with two Gaussians peaking at $Z = 52.2$ and 56.5, with the neutron-excessive curve accounting for some 40% of the total isobaric yield of 23.3 ± 0.4 mb. The two curves overlap to a substantial extent, the peak-to-valley ratio being 2 to 1 and the minimum occurring just at the line of β stability.

The recoil ranges have values characteristic of binary fission up to cesium, at which point a factor-of-2 decrease occurs over an interval of $2Z$ units. The transition point between long and short ranges occurs some $2Z$ units higher than the mini-

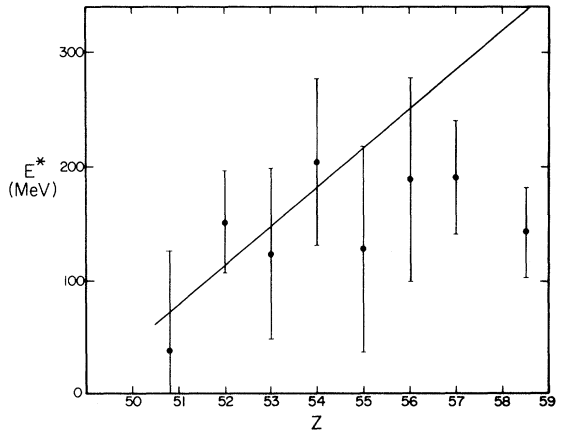

FIG. 8. Variation of deposition energy with product Z. The solid line shows a 35 MeV/Z increase obtained in 450-MeV fission (Ref. 9).

mum between the two peaks in the charge dispersion. This difference can be explained if the charge dispersion does not, in fact, consist of two Gaussians but of a broad and highly asymmetric neutron-excessive peak and a narrower neutron-deficient peak. Alternatively, a charge dispersion consisting of two Gaussian-like curves leads to the conclusion that fission is the principal mechanism on the neutron-rich side of the neutron-deficient peak as well as over the entire neutron-excessive peak. The minimum in the charge dispersion would then reflect a reduction in the probability of fission events leading to products near stability relative to those leading to more neutron-excessive and -deficient products. The reason for such a reduction remains obscure although it is presumably connected to the details of the distribution of residual nuclei following the prompt cascade as well as to the ensuing competition between spallation and fission.

Various attempts have been made to transform the isotopic distribution of cesium yields into an isobaric distribution at $A = 131$. Comparison with the present results indicates that none of the approaches used is very satisfactory. It does appear, however, that better agreement with experiment is obtained when the effects of shell closure on Z_A values are ignored by the use of N/Z rather than $Z_A - Z$ as the composition variable.

The continued assistance of Dr. E. Steinberg with the ZGS irradiations is gratefully acknowledged. We would like to thank Dr. G. Friedlander and Miss E. M. Franz for making the AGS irradiations possible.

---

*Work supported by the U. S. Atomic Energy Comission.

[1]S. Kaufman, Phys. Rev. 129, 1866 (1963).
[2]N. T. Porile, Phys. Rev. 148, 1235 (1966).
[3]J. A. Panontin and N. T. Porile, J. Inorg. Nucl. Chem. 32, 1775 (1970).
[4]E. Hagebø, J. Inorg. Nucl. Chem. 32, 2489 (1970).
[5]G. Friedlander, L. Friedman, B. Gordon, and L. Yaffe, Phys. Rev. 129, 1809 (1963).
[6]G. Friedlander, in *Proceedings of the Symposium on the Physics and Chemistry of Fission, Salzburg, 1965* (International Atomic Energy Agency, Vienna, Austria, 1965), Vol. II, p. 265.
[7]Y. Y. Chu, E. M. Franz, G. Friedlander, and P. J. Karol, Phys. Rev. C 4, 2202 (1971).
[8]J. A. Panontin and N. T. Porile, J. Inorg. Nucl. Chem. 30, 2017 (1968).
[9]J. J. Hogan and N. Sugarman, Phys. Rev. 182, 1210 (1969).
[10]A. C. Pappas and E. Hagebø, J. Inorg. Nucl. Chem. 28, 1769 (1966).
[11]J. A. Panontin and N. Sugarman, J. Inorg. Nucl. Chem. 34, 1485 (1972).
[12]N. Sugarman, M. Campos, and K. Wielgoz, Phys. Rev. 101, 388 (1956).
[13]J. Alexander, C. Baltzinger, and M. F. Gadzik, Phys. Rev. 129, 1826 (1963).
[14]R. Brandt, in *Proceedings of the Symposium on the Physics and Chemistry of Fission, Salzburg, 1965* (see Ref. 6), Vol. II, p. 329.
[15]E. Hagebø and H. Ravn, J. Inorg. Nucl. Chem. 31, 2649 (1969).
[16]K. Beg and N. T. Porile, Phys. Rev. C 3, 1631 (1971).
[17]J. B. Cumming and K. Bächmann, Phys. Rev. C 6, 1362 (1972).
[18]N. Sugarman, H. Munzel, J. A. Panontin, K. Wielgoz, M. V. Ramanaiah, G. Lange, and E. Lopez-Menchero, Phys. Rev. 143, 952 (1966).
[19]J. A. Panontin and N. T. Porile, J. Inorg. Nucl. Chem. 30, 2027 (1968).
[20]V. P. Crespo, J. B. Cumming, and A. M. Poskanzer, Phys. Rev. 174, 1455 (1968).
[21]K. Bächmann and J. B. Cumming, Phys. Rev. C 5, 210 (1972).
[22]A. E. Norris, G. Friedlander, and E. M. Franz, Nucl. Phys. 86, 102 (1966).
[23]N. T. Porile, Yu-Wen Yu, O. A. Schaeffer, and R. Warasila, to be published.
[24]J. Hudis, T. Kirsten, R. W. Stoenner, and O. A. Schaeffer, Phys. Rev. C 1, 2019 (1970).
[25]C. M. Lederer, J. M. Hollander, and I. Perlman, *Table of Isotopes* (Wiley, New York, 1967), 6th ed.
[26]J. B. Cumming, National Academy of Sciences Report No. NAS-NS-3107, 1962 (unpublished), p. 25.
[27]J. B. Cumming, Ann. Rev. Nucl. Sci. 13, 261 (1963).
[28]A. F. Stehney and E. P. Steinberg, Nucl. Instr. Methods 59, 102 (1968).
[29]R. Brandt, Ch. Gfeller, and W. Stotzel-Riezler, Nucl. Instr. Methods 62, 109 (1968).
[30]Y. Y. Chu, E. M. Franz, and G. Friedlander, Nucl. Phys. B40, 428 (1972).
[31]E. Hagebø, J. Inorg. Nucl. Chem. 29, 2515 (1967).
[32]G. Rudstam and G. Sørensen, J. Inorg. Nucl. Chem. 28, 771 (1966).
[33]J. Chaumont, Ph.D. thesis, University of Paris, 1970 (unpublished).
[34]P. Starzyk and N. Sugarman, private communication.
[35]N. T. Porile, Phys. Rev. 185, 1371 (1969).
[36]V. P. Crespo, J. M. Alexander, and E. K. Hyde, Phys. Rev. 131, 1765 (1963).